Korean J. Chem. Eng., 35(5), 1083-1088 (2018)
DOI: 10.1007/s11814-018-0015-y

pISSN: 0256-1115
eISSN: 1975-7220

Influence of calcination temperature on the structure and properties of Al_2O_3 as support for Pd catalyst

Mi Yeon Byun*,, Ji Sun Kim***, Dae-Won Park**,†, and Man Sig Lee*,†**

*Ulsan Regional Division, Korea Institute of Industrial Technology (KITECH), Ulsan 44413, Korea
**Department of Polymer Science and Chemical Engineering, Pusan National University, Busan 46241, Korea
***Department of Chemical & Biological Engineering, The University of British Columbia, Vancouver, BC, Canada
(*Received 19 October 2017 • accepted 2 February 2018*)

Abstract−We investigated the influence of the calcination temperature on the structural properties of Al_2O_3 and how the resultant Al_2O_3 support affects the characteristics of Pd/Al_2O_3 catalysts. Al_2O_3 pretreated at different calcination temperatures ranging from 500 °C to 1,150 °C, was used as catalyst supports. The Pd/Al_2O_3 catalysts were prepared by a deposition-precipitation method using a pH 7.5 precursor solution. Characterization of the prepared Pd/Al_2O_3 catalysts was performed by X-ray diffraction (XRD), N_2-physisorption, CO_2-temperature programmed desorption (TPD), CO-chemisorption, and field emission-transmission electron microscopic (FE-TEM) analyses. The CO-chemisorption results showed that the Pd catalyst with the Al_2O_3 support calcined at 900 °C, Pd/Al_2O_3 (900), had the highest and most uniformly dispersed Pd particles, with a Pd dispersion of 29.8%. The results suggest that the particle size and distribution of Pd are related to the phase transition of Al_2O_3 and the ratio of isolated tetrahedral to condensed octahedral coordination sites (i.e., functional groups), where the tetrahedral sites coordinate more favorably with Pd.

Keywords: Aluminum Oxide, Deposition-precipitation, Functional Group, Palladium Nanoparticle, Phase Transition

INTRODUCTION

The petrochemical industry has always exploited catalysts in order to improve the activity and selectivity for reaction, keeping energy usage, and costs down. In particular, platinum-group metals (PGMs), which include platinum, palladium, rhodium, ruthenium, iridium, and osmium, have attracted much attention in the hydrogenation and dehydrogenation processes of the petroleum chemistry due to their enhanced activity/selectivity, high melting point, and stability to oxidation [1-3]. However, PGMs are expensive and rare materials. Thus, to reduce cost, small quantities of PGMs are often dispersed on supports with a large specific surface area. Commonly used supports include Al_2O_3, SiO_2, TiO_2, carbon, and zeolite materials. Among these, Al_2O_3 has a wide variety of applications due to its phase transitions, thermal stability, specific surface area, surface characteristics (acidity, basicity), and mechanical properties, all of which play an important role in influencing the catalyst and support properties [4-6]. Especially, the Pd/Al_2O_3 catalyst has been widely used in the chemical industry. Several researchers reported that Pd/Al_2O_3 catalyst exhibited catalytic performance in hydrogenation, selective hydrogenation, methane oxidation, and CO-oxidation reaction [7-10]. Al_2O_3 is formed by heat treatment of aluminum hydroxide. Aluminum hydroxides are classified as boehmite, bayerite, diaspore, and gibbsite. The structure of these aluminum hydroxides is determined by the rate of solubilization and crystallization during synthesis [5]. Depending on the types of aluminum hydroxide present, Al_2O_3 can consist of α, β, γ, δ, θ, or χ phases [6]. Among them, γ-Al_2O_3 is the most widely used as catalyst, catalyst support, and ion exchanger [11]. For example, γ-Al_2O_3 provides a high specific surface area, high porosity, and a higher number of surface active sites than the other phases. Especially, it is widely used as a support for preparing highly dispersed Pd and Pt noble metal catalysts. However, when γ-Al_2O_3 is calcined at temperatures above 1,000 °C, the $\gamma \rightarrow \theta \rightarrow \alpha$ phase transition occurs and the specific surface area and pore volume decrease drastically, while the particle size increases dramatically. The phase transitions and structural properties of Al_2O_3 are widely studied. Yuan et al. reported that the structure of boehmite consists of tetrahedral (AlO_4), pentahedral (AlO_5), and octahedral (AlO_6) coordination sites; however, upon calcination above 900 °C, pentahedrally coordinated alumina disappears and boehmite is transformed to the γ-Al_2O_3 phase [12]. Kwak et al. reported that the amount of pentahedrally coordinated alumina is a crucial factor in improving the thermal stability of γ-Al_2O_3 and inhibiting the phase transition of γ-Al_2O_3 to θ-Al_2O_3 [13]. Other researchers have also studied the effect of metal interactions with the surface functional groups of Al_2O_3 on the characteristics of the catalyst. Based on Fourier transform infrared (FT-IR) analysis, Marsala et al. reported that Al_2O_3 surfaces have functional groups such as =Al-O and =Al-OH; these groups undergo electrostatic attraction and ion-exchange with metal ions [14]. Belskaya et al. investigated the interactions between metal precursors and the Al_2O_3 support, demonstrating that the interactions were affected by the ratio of the aluminum atoms coordinated to hydroxyl groups in various modes [15]. Recent studies have shown that it is possible to prepare highly dispersed noble metals supported on Al_2O_3 by using

†To whom correspondence should be addressed.
E-mail: lms5440@kitech.re.kr, dwpark@pusan.ac.kr

different catalyst preparation methods, reducing agents, and ordered mesoporous alumina. However, only a few studies have discussed the effect of the structure and surface functional groups of Al_2O_3 on the particle size and distribution of Pd. Herein, we investigate Al_2O_3, modified by calcination at various temperatures, and their influence on the characteristics of Pd/Al_2O_3 catalysts. The prepared Al_2O_3 supports and Pd/Al_2O_3 catalysts are characterized using X-ray diffraction (XRD), N_2-physisorption, CO_2-temperature programmed desorption (TPD), and FT-IR spectroscopy. The Pd/Al_2O_3 catalysts are further characterized using CO-chemisorption and field emission-transmission electron microscopy (FE-TEM). Using this approach, we demonstrate that the characteristics of the Pd/Al_2O_3 catalyst are influenced by the morphology of Al_2O_3 as well as the surface functional groups.

EXPERIMENTAL

1. Materials

Commercially prepared Al_2O_3 (≥99%, γ phase, average particle size: 20 nm) was purchased from Alfa-Aesar. Formalin solution (10 wt%), hydrochloric acid (HCl, 38%), palladium(II) chloride ($PdCl_2$, 90%), and sodium hydroxide (NaOH, ≥99.0%) were purchased from Sigma Aldrich. The Pd precursor solution was prepared by dissolving 0.1 mol of $PdCl_2$ in 0.2 M HCl with vigorous stirring for 24 h.

2. Support Pretreatment

Al_2O_3 was calcined at temperatures of 500, 900, 1,100, and 1,150 °C for 4 h in air. The Al_2O_3 support prepared without calcination is denoted as Al_2O_3 (105), whereas the calcined supports are reported with their calcination temperature, e.g., Al_2O_3 (900).

3. Catalyst Preparation

Catalysts containing 5 wt% of Pd supported on Al_2O_3 were prepared by using a deposition-precipitation method. An aqueous solution of the Pd precursor was heated to 60 °C and Al_2O_3 was then added to the solution. The precursor solution was adjusted to a pH=7.5 by adding NaOH solution to precipitate the metal precursor. The solution was stirred for 3 h. Reduction of the catalyst was carried out in the liquid phase by treatment with formalin at 85 °C for 3 h. The solid was then filtered and washed with deionized water. All catalysts were dried at 105 °C for 24 h.

4. Characterization

The crystal structures were analyzed by X-ray diffraction (XRD) using an X'Pert-MPD (Philips, Netherlands) instrument with a Cu-Kα radiation source (1.5405 Å) operating at a voltage of 40 kV and a current of 30 mA. The XRD patterns of both the catalyst and supports were collected in the 2θ range of 5-90° at a scan rate of 0.9° min^{-1}. Characterization of the physical properties of each sample was performed using nitrogen adsorption/desorption isotherms. The nitrogen sorption isotherm was measured at −196 °C on an ASAP 2020 (Micromeritics, USA) instrument. Before the measurement, the samples were degassed under vacuum at 150 °C for 6 h. The Brunauer-Emmett-Teller (BET) method was used to estimate the specific surface area. The pore volume and pore size were calculated using the Barrett-Joyner-Halenda (BJH) method. The basicity of the supports was analyzed by CO_2 temperature programmed desorption (TPD) using an AutoChem 2920 (Micromeritics, USA) instrument. The sample (0.1 g) in a U-shape quartz reactor was pretreated with 5% H_2/He at a flow rate of 20 mL min^{-1} and then heated to 600 °C and maintained for 1 h under Ar at a flow rate of 20 mL min^{-1}. The functional groups on the catalyst supports were analyzed by Fourier transform infrared spectroscopy (FT-IR) in the range of 4,000-400 cm^{-1} using the KBr pellet method. The FT-IR spectra were obtained with a Frontier (Perkin-Elmer, USA) IR instrument. The amount of Pd active sites and the dispersion of Pd were determined by the CO-pulse chemisorption technique using an AutoChem 2920 (Micromeritics, USA) instrument. Briefly, 0.1 g of sample was charged into a U-shaped quartz reactor and was reduced under a flow of H_2/Ar at 200 °C for 1 h. A CO pulse (10% CO/Ar) was injected into the catalyst at 50 °C. The amount of adsorbed CO was determined by assuming a stoichiometry of one CO molecule for two surface Pd atoms [16]. The dispersion and crystallite size of Pd were calculated using Eqs. (2.1) and (2.1a).

$$\text{Metal dispersion} = \frac{\text{Chemisorption Site}}{\text{Metal Atomicity}} \times 100 \quad (2.1)$$

$$= \frac{\text{Vchem} \cdot \text{SF} \cdot \text{Mw}}{\text{C}/100} \times 100 \quad (2.1a)$$

V_{chem}: CO chemisorption volume, M_w: Pd atomic weight, SF: stoichiometry factor, and C/100: supported metal weight.

RESULTS AND DISCUSSION

Fig. 1 shows the XRD patterns of the Al_2O_3 supports treated at different temperatures. When the Al_2O_3 supports were heat treated to 900 °C, Al_2O_3 (105), Al_2O_3 (500), and Al_2O_3 (900) showed only the γ phase in the XRD spectra. However, with an increase in the calcination temperature from 900 °C to 1,100 °C, the Al_2O_3 support underwent a $\gamma \rightarrow \theta$ phase transition. Al_2O_3 (1100) comprised a mix of θ and α phases, whereas Al_2O_3 (1150) comprised the pure α phase. From the XRD analysis, 900 °C was identified as the beginning of the phase transition, and α-Al_2O_3 was formed as a final product of Al_2O_3 calcined at 1,150 °C due to dehydration and heat

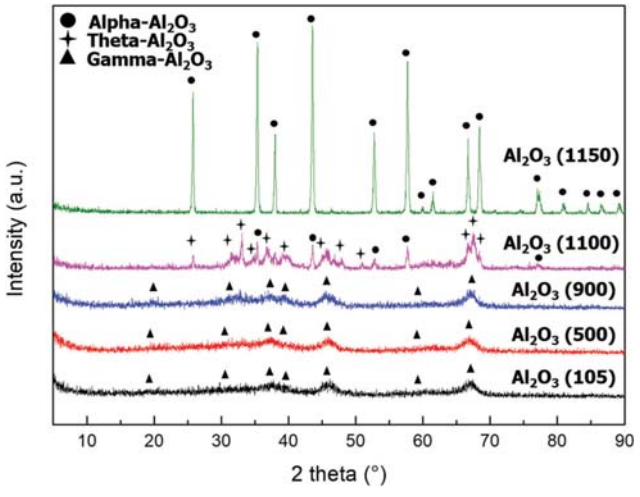

Fig. 1. XRD patterns of the Al_2O_3 supports treated at different calcination temperatures.

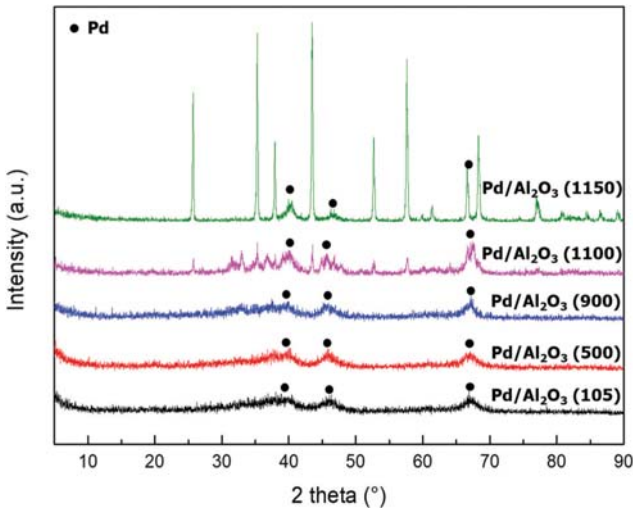

Fig. 2. XRD patterns of Pd/Al_2O_3 catalysts prepared with Al_2O_3 calcined at various temperature.

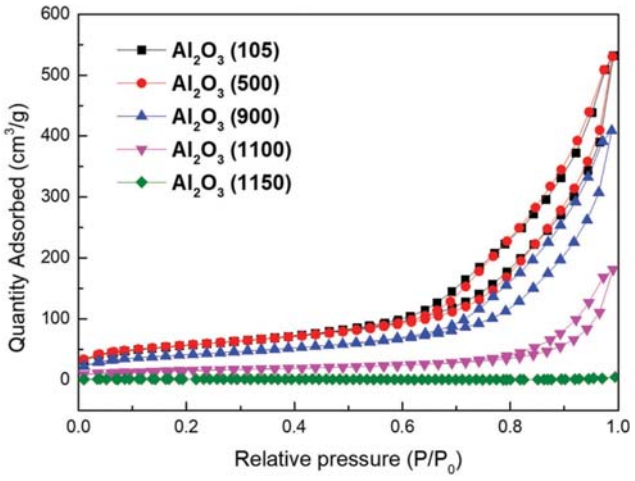

Fig. 3. Nitrogen adsorption and desorption isotherms of Al_2O_3 supports.

Table 1. Physical properties of Al_2O_3 supports

Support	Specific surface area (m^2/g)	Pore volume (cm^3/g)[a]	Pore size (nm)[a]
Al_2O_3 (105)	195	0.82	13.1
Al_2O_3 (500)	199	0.82	13.2
Al_2O_3 (900)	146	0.62	14.4
Al_2O_3 (1100)	54	0.28	21.5
Al_2O_3 (1150)	6	0.007	32.9

[a]Base on BJH method

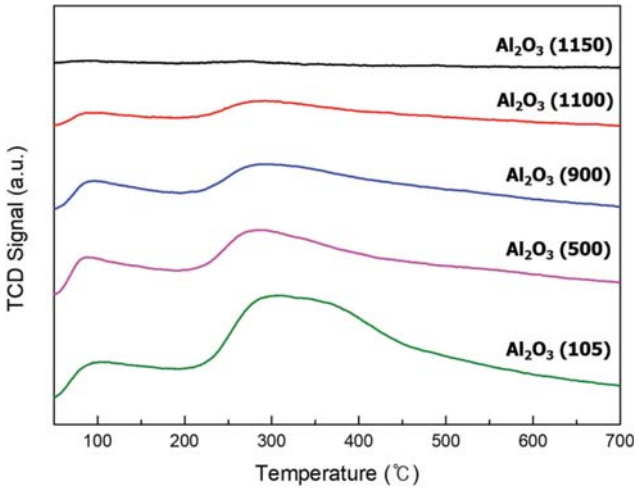

Fig. 4. CO_2-TPD profiles of Al_2O_3 supports.

treatment. For the Pd/Al_2O_3 catalysts (Fig. 2), characteristic XRD peaks were observed at 2θ=40.11°, 46.6°, and 68.08°, originating from Pd.

Table 1 presents a summary of the physical properties of Al_2O_3, including the specific surface area and pore volume. For the Al_2O_3 supports calcined at temperatures less than or equal to 900 °C, the specific surface area and total pore volume decreased slightly from 195 $m^2\ g^{-1}$ to 146 $m^2\ g^{-1}$ and 0.82 $cm^3\ g^{-1}$ to 0.62 $cm^3\ g^{-1}$, respectively. However, for the Al_2O_3 supports calcined over 900 °C, the specific surface area and total pore volume decreased dramatically from 146 $m^2\ g^{-1}$ to 6 $m^2\ g^{-1}$ and 0.62 $cm^3\ g^{-1}$ to 0.007 $cm^3\ g^{-1}$, respectively. The pore size of Al_2O_3 calcined at temperatures up to 900 °C was in the range of 13.1-14.4 nm. However, the pore size of Al_2O_3 calcined over 900 °C gradually increased from 14.4 nm to 32.9 nm. The extreme decrease in the specific surface area and total pore volume can be explained by the $\gamma \rightarrow \theta$ and α phase transition.

Fig. 3 shows the nitrogen adsorption and desorption isotherms of the Al_2O_3 catalyst supports. According to the IUPAC classification, the Al_2O_3 (105), Al_2O_3 (500), Al_2O_3 (900), and Al_2O_3 (1100) supports showed type-IV isotherms with a H1 hysteresis loop, which is a typical feature of mesoporous materials [17]. The capillary condensation of Al_2O_3 (105), Al_2O_3 (500), and Al_2O_3 (900) was initiated at a relative pressure (P/P_0) ranging from 0.6 to 0.7, whereas capillary condensation of Al_2O_3 (1100) occurred at a relative pressure of 0.8, indicating an increase in the pore size. When the calcination temperature increased to 1,100 °C, the areas of the hysteresis loops decreased and the pore size increased. However, the Al_2O_3 (1150) support showed a type-III isotherm, representing a nonporous material, which indicates that the pore volume decreased dramatically due to the phase transition [18].

The basic properties of Al_2O_3 were studied by CO_2-TPD as shown in Fig. 4. The Al_2O_3 supports showed two desorption peaks at 100 °C and 300 °C, corresponding to weakly basic sites and medium/strongly basic sites, respectively. When the Al_2O_3 support was heat treated up to 500 °C, the number of weakly basic sites and medium/strongly basic sites decreased remarkably. It appears that the weakly and medium/strongly basic sites of the Al_2O_3 supports gradually decreased as the calcination temperature increased from 500 °C to 1,100 °C. However, the desorption peak of CO_2 for Al_2O_3 calcined over 1,100 °C had the lowest intensity due to the phase transition of Al_2O_3.

To observe the change in the surface functional groups of Al_2O_3 as a function of heat treatment, the supports were analyzed by FT-IR, as shown in Fig. 5. The absorption bands observed at 3,500

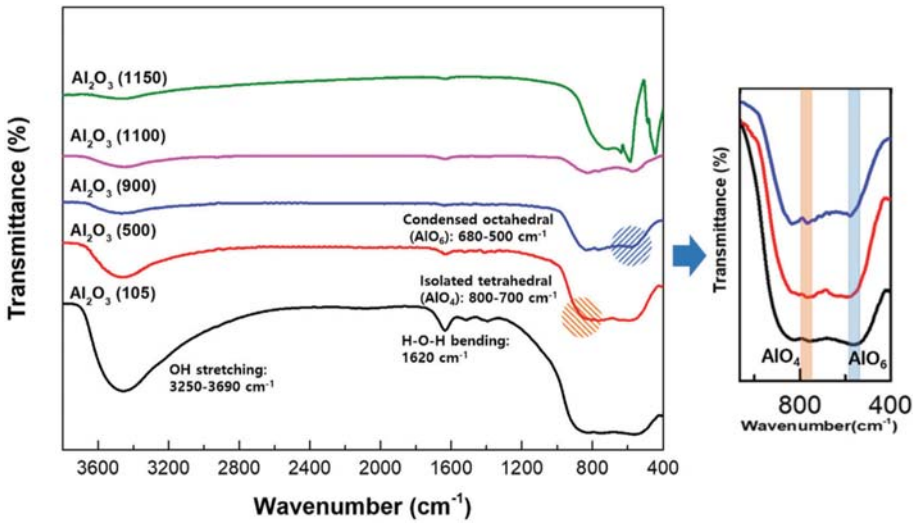

Fig. 5. FT-IR spectra of Al_2O_3 supports.

cm^{-1} and 1,600 cm^{-1} were assigned to -OH stretching and H-O-H bending, respectively [19]. As the calcination temperature increased, the intensity of the -OH stretching and H-O-H bending bands decreased as the hydroxyl groups on Al_2O_3 gradually disappeared. The other adsorption bands at 800-650 cm^{-1} and 680-500 cm^{-1} correspond to AlO_4 (isolated tetrahedral) and AlO_6 (condensed octahedral), respectively [6,15,20]. The FT-IR spectra show that the ratio of AlO_4 to AlO_6 changed with an increase in the calcination temperature. It can be seen that the ratio of AlO_4 to AlO_6 increased as the calcination temperature increased from 500 °C to 900 °C. However, for calcination temperatures above 900 °C, the AlO_4 to AlO_6 ratio gradually decreased, eventually giving rise to a strong peak indicating the presence of AlO_6 (condensed octahedral) [21]. These results indicate that the ratio of AlO_4 to AlO_6 functional groups changed during the phase transition of Al_2O_3.

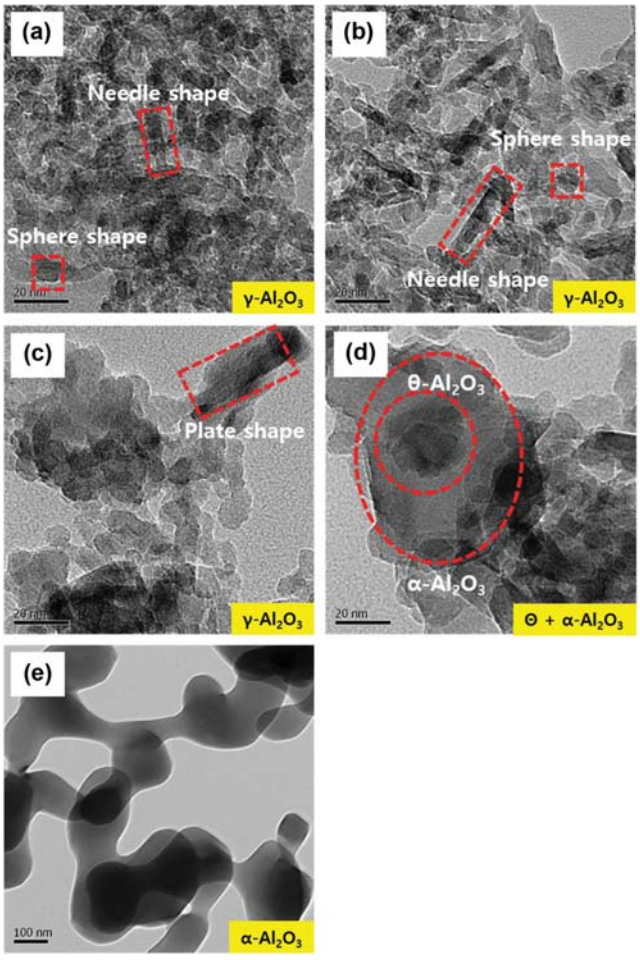

Fig. 6. FE-TEM images of Al_2O_3; (a) Al_2O_3 (105), (b) Al_2O_3 (500), (c) Al_2O_3 (900), (d) Al_2O_3 (1100), and (e) Al_2O_3 (1150).

Fig. 6 shows the FE-TEM images of Al_2O_3 treated at different temperatures. The Al_2O_3 (105) and Al_2O_3 (500) supports had spherical and needle-like particle morphologies, whereas Al_2O_3 (900) appeared to comprise plate-like structures. The FE-TEM images reveal that Al_2O_3 (105), Al_2O_3 (500), and Al_2O_3 (900) possessed similar structures, corresponding to the γ-Al_2O_3 phase. In the case of Al_2O_3 (1100), some particles with a larger size were observed due to sintering between particles at high temperatures. The XRD analysis confirmed that Al_2O_3 (1100) comprised a mixture of θ and α phases. The FE-TEM image showed different particle sizes, corresponding to the θ-Al_2O_3 and α-Al_2O_3 phases. However, Al_2O_3 (1150) showed a dramatic increase in the particle size, related to the θ-$Al_2O_3 \rightarrow \alpha$-$Al_2O_3$ phase transition. The FE-TEM images of Al_2O_3 agree with the XRD and N_2 adsorption-desorption data.

The results of the CO-chemisorption experiments are summarized in Table 2. The Pd/Al_2O_3 (900) catalyst had the highest Pd dispersion of 29.8%, whereas the Pd/Al_2O_3 (1150) catalyst had the lowest Pd dispersion of 2.9%. These results can be explained from two perspectives: the structure and surface functional groups. γ-Al_2O_3 is widely used as a catalyst support due to its high specific surface area and large number of active sites. Consequently, when the Al_2O_3 support comprises the γ phase, Pd is well dispersed on Al_2O_3. The Al_2O_3 (105), Al_2O_3 (500), and Al_2O_3 (900) supports have an intact surface area and high number of active sites. However, the Al_2O_3 (1100) and Al_2O_3 (1150) supports had a relatively

Table 2. CO-chemisorption results of Pd/Al_2O_3 catalysts

Catalyst	Metal dispersion (%)	Cumulative quantity (mmol/g)	Metallic surface area (m^2/g)
Pd/Al_2O_3 (105)	20.6	0.048	91.6
Pd/Al_2O_3 (500)	20.8	0.049	92.7
Pd/Al_2O_3 (900)	29.8	0.070	132.8
Pd/Al_2O_3 (1100)	11.0	0.026	48.9
Pd/Al_2O_3 (1150)	2.90	0.00068	12.9

low specific surface area and fewer active sites due to the characteristics of the θ and α phases, accounting for why the Pd dispersion was lower for the Pd/Al_2O_3 (1100) and Pd/Al_2O_3 (1150) catalysts. The Pd/Al_2O_3 (1150) catalyst showed the lowest Pd dispersion of 2.9% because the Al_2O_3 (1150) support comprises only the α phase with weakly basic sites. The low specific surface area and weak basicity of the α phase lead to low dispersion of Pd. On the other hand, Al_2O_3 (105) and Al_2O_3 (500) had a higher specific surface area and stronger basic sites than Al_2O_3 (900), as determined by the N_2 adsorption-desorption and CO_2-TPD analyses. Nevertheless, the Pd dispersion was higher for the Pd/Al_2O_3 (900) catalyst than the Pd/Al_2O_3 (105) and Pd/Al_2O_3 (500) catalysts. We suggest that the ratio of functional groups on Al_2O_3 affects the Pd particle size and distribution. FT-IR analysis confirmed that the ratio of AlO_4 to AlO_6 changed based on the calcination temperature. Al_2O_3 (900) had a relatively higher AlO_4 to AlO_6 ratio than Al_2O_3 (105) and Al_2O_3 (500), for which the content of AlO_4 and AlO_6 was more even. Fig. 8 shows the structure of isolated tetrahedral and condensed octahedral in the Al_2O_3 lattice [22]. It is well known that γ-Al_2O_3 consists of unstable tetrahedrally coordinated species and octahedrally coordinated species. The catalyst was prepared by the deposition-precipitation method using $PdCl_2$ as the Pd precursor. The $PdCl_2$ precursor is present as the $PdCl_4^{2-}$ anion in an acid solution and anion exchange occurs between OH groups on the Al_2O_3 surface and the $PdCl_4^{2-}$ anion [23,24]. During the deposition-precipitation process, $Pd(OH)_2$ was formed on the surface of Al_2O_3 upon the addition of NaOH. Prior to the formation of $Pd(OH)_2$, the electrostatic attraction between Al_2O_3 and the Pd precursor plays an important role in determining the particle size and distribution of Pd. Preudhomme et al. reported that the isolated tetrahedra do not share a common oxygen between tetrahedra and that the condensed octahedra share common oxygen groups at the edges [22]. Additionally, M. Trueba et al. reported that the tetrahedral cation is regarded as a strongly acidic site [25]. Marquez et al. reported that strongly acidic site of tetrahedral cation was associated with strong metal-support interaction between Pd and Al_2O_3 [26].

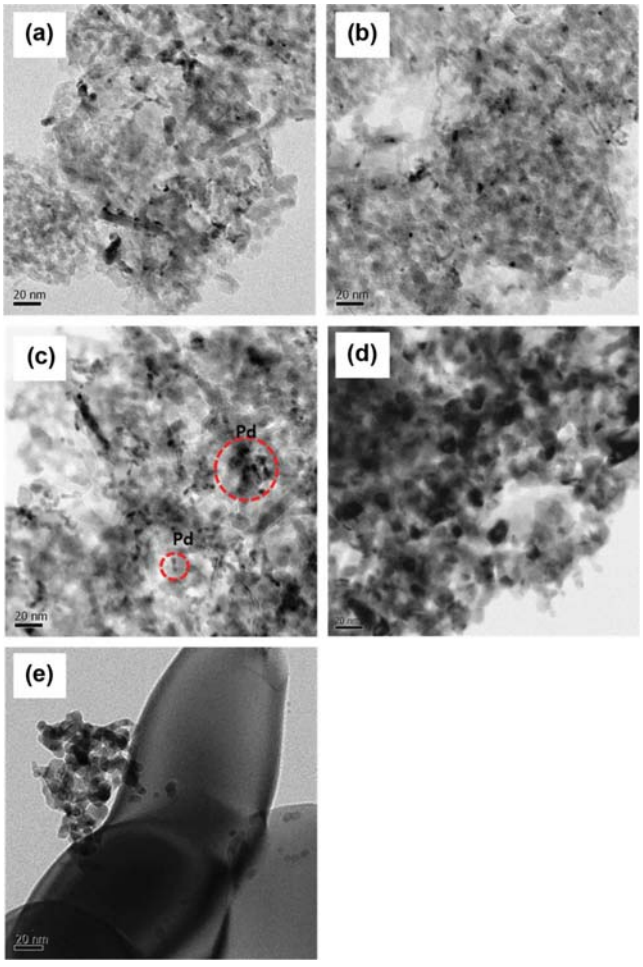

Fig. 7. FE-TEM images of Pd/Al_2O_3; (a) Pd/Al_2O_3 (105), (b) Pd/Al_2O_3 (500), (c) Pd/Al_2O_3 (900), (d) Pd/Al_2O_3 (1100), and (e) Pd/Al_2O_3 (1150).

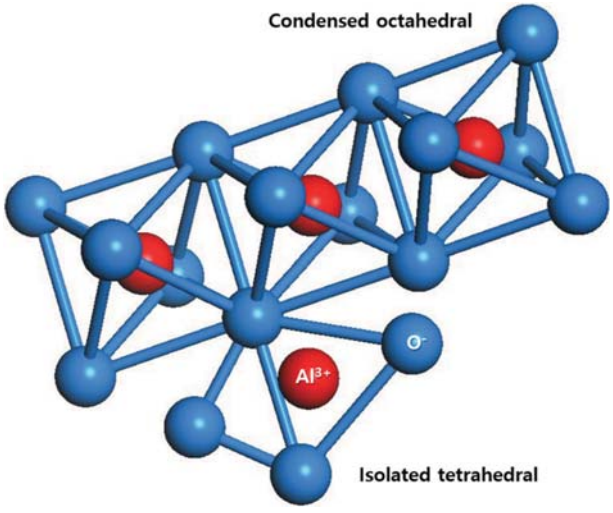

Fig. 8. Isolated tetrahedral and condensed octahedral structure in the Al_2O_3 lattice [14].

With respect to the interactions of Pd and Al_2O_3, the more unstable the Al_2O_3 site, the better the interaction between Pd and Al_2O_3. Because Al_2O_3 (900) has a larger ratio of unstable isolated tetrahedral sites than Al_2O_3 (105) and Al_2O_3 (500), Pd is well dispersed on Al_2O_3 and the particle size is small.

To confirm the particle size and distribution of Pd, FE-TEM images of the Pd/Al_2O_3 catalysts are shown in Fig. 7. The Pd/Al_2O_3 (900) catalyst had the smallest Pd particles, and the particles were well dispersed on Al_2O_3. However, in the case of the Pd/Al_2O_3 (1100) catalyst, the Pd particles were larger than those of Pd/Al_2O_3 (900) due to the phase transition of Al_2O_3. Finally, the Pd/Al_2O_3 (1150) catalyst comprised the α phase, thus Pd was not well dispersed on Al_2O_3. The FE-TEM images of the Pd/Al_2O_3 catalysts agree with the CO-chemisorption results.

CONCLUSIONS

We investigated the effect of the calcination temperature on the physical and chemical properties of Al_2O_3, including the particle size and distribution of Pd. The γ phase was preserved for the Al_2O_3 supports calcined at temperatures up to 900 °C, with a high specific surface area and a large number of active sites. When the Al_2O_3 support comprised only the γ phase, the ratio of AlO_4 (isolated tetrahedral) to AlO_6 (condensed octahedral) in the structure changed depending on the calcination temperature. We suggest that the higher the ratio of unstable AlO_4, the better the interaction between Pd and Al_2O_3. Calcination of Al_2O_3 at 900 °C preserved the γ phase and the ratio of AlO_4 to AlO_6 was higher than achieved at other temperatures. These features are associated with the highest Pd dispersion (29.8%) and the smallest particle size (10-20 nm) observed for the Pd/Al_2O_3 (900) catalyst.

ACKNOWLEDGEMENTS

This research was financially supported by DR AXION CO. (Project No. IR170027) and Korea Institute of Industrial Technology (KITECH) (Project No. JA180001).

REFERENCES

1. C. R. M. Rao and G. S. Reddi, *TrAC- Trends Anal. Chem.*, **19**, 565 (2000).
2. J. S. Kim, J. H. Baek, Y. B. Ry, S.-S. Hong and M. S. Lee, *J. Nanosci. Nanotechnol.*, **15**, 290 (2015).
3. J. S. Kim, J.-W. Park, S.-S. Hong and M. S. Lee, *Sci. Adv. Mater.*, **8**, 1995 (2016).
4. T. Shirai, H. Watanabe, M. Fuji and M. Takahashi, *Annu. Rep. Adv. Ceram. Res. Cent. Nagoya Inst. Technol.*, **9**, 23 (2009).
5. G. Paglia, C. E. Buckley, A. L. Rohl, R. D. Hart, K. Winter, A. J. Studer, B. A. Hunter and J. V. Hanna, *Chem. Mater.*, **16**, 220 (2004).
6. M. F. Peintinger, M. J. Kratz and T. Bredow, *J. Mater. Chem. A*, **2**, 13143 (2014).
7. M. Haneda, M. Todo, Y. Nakamura and M. Hattori, *Catal. Today*, **281**, 447 (2017).
8. P. A. Carlsson, E. Fridell and M. Skoglundh, *Catal. Lett.*, **115**, 1 (2007).
9. K. Pattamakomsan, K. Suriye, S. Dokjampa, N. Mongkolsiri, P. Praserthdam and J. Panpranot, *Catal. Commun.*, **11**, 311 (2010).
10. S. Komhom, O. Mekasuwandumrong, P. Praserthdam and J. Panpranot, *Catal. Commun.*, **10**, 86 (2008).
11. J. M. Saniger, *Mater. Lett.*, **22**, 109 (1995).
12. Q. Yuan, A.-X. Yin, C. Luo, L.-D. Sun, Y.-W. Zhang, W.-T. Duan, H.-C. Liu and C.-H. Yan, *J. Am. Chem. Soc.*, **130**, 3465 (2008).
13. J. H. Kwak, C. H. F. Peden and J. Szanyi, *J. Phys. Chem. C*, **115**, 12575 (2011).
14. A. Amirsalari and S. Farjami Shayesteh, *Superlattices Microstruct.*, **82**, 507 (2013).
15. O. B. Belskaya, I. G. Danilova, M. O. Kazakov, R. M. Mironenko, A. V. Lavrenov and V. a. Likholobov, *ChemInform.*, **44**, 149 (2013).
16. P. Canton, G. Fagherazzi, M. Battagliarin, F. Menegazzo, F. Pinna and N. Pernicone, *Langmuir.*, **18**, 6530 (2002).
17. Q. Wu, F. Zhang, J. Yang, Q. Li, B. Tu and D. Zhao, *Micropor. Mesopor. Mater.*, **143**, 406 (2011).
18. D. Li, C. Wu, P. Tang and Y. Feng, *Mater. Lett.*, **133**, 278 (2014).
19. J. Gangwar, B. K. Gupta, P. Kumar, S. K. Tripathi and A. K. Srivastava, *Dalton Trans.*, **43**, 17034 (2014).
20. P. Tarte, *Spectrochim. Acta Part A Mol. Spectrosc.*, **23**, 2127 (1967).
21. J. Gangwar, K. K. Dey, Komal, Praveen, S. K. Tripathi and A. K. Srivastava, *Adv. Mater. Lett.*, **2**, 402 (2011).
22. J. Preudhomme and P. Tarte, *Acta Part A Mol. Spectrosc.*, **27**, 845 (1971).
23. K. Ito, M. Ohshima, H. Kurokawa, K. Sugiyama and H. Kurokawa, *Catal. Commun.*, **3**, 527 (2002).
24. I. Balint, A. Miyazaki and K. I. Aika, *Chem. Mater.*, **13**, 932 (2001).
25. M. Trueba and S. P. Trasatti, *Eur. J. Inorg. Chem.*, **17**, 3393 (2005).
26. A. M. Márquez anf J. F. Sanz, *Appl. Surf. Sci.*, **238**, 82 (2004).